Soil Salinity Inversion Model Based on BPNN Optimization Algorithm for UAV Multispectral Remote Sensing

Wenju Zhao, Hong Ma, Chun Zhou, Changquan Zhou, and Zongli Li, *Member, IEEE*

***Abstract*—Rapid and accurate inversion of soil salinity is a key scientific problem that needs to be solved urgently. Due to the accuracy of UAV multispectral remote sensing inversion of salinity based on back propagation neural network (BPNN) is low, in this study, used the UAV multispectral image and field measurements of 60 soil surface salinity as data sources, 16 salinity indexs were constructed using the extracted spectral reflectance, and performed a gray relation analysis to screen salinity index features after applying a film removal to construct the BPNN salinity inversion model. Particle swarm optimization (PSO), thinking evolutionary algorithm (MEA), and genetic algorithm (GA) were applied to optimize the BPNN inverse model, respectively, and the optimization capabilities of the four algorithms were compared and evaluated to optimize the best optimization algorithm. The results showed that the GRA variable screening can effectively remove the redundant information of spectral parameters and reduce the complexity of the salinity inversion model; the PSO, MEA, and GA can effectively improve the robusticity of BPNN inversion model, and GA algorithm has the best optimization effect in terms of inverse model optimization effect, followed by MEA and PSO algorithms; the accuracy of the PSO-BPNN, MEA-BPNN, and GA-BPNN inversion models are better than that of the BPNN model, and GA-BPNN is the best salinity inversion model, which achieves R^2 of 0.6659, RMSE of 0.0751, and RPD of 2.0211. This approach can effectively solve salinity monitoring accuracy issues of UAV multispectral inversion.**

***Index Terms*—Inversion model, optimistic algorithm, soil salinity, UAV multispectral, variable screening.**

I. Introduction

SOIL salinization is one of the significant soil degradation problems especially faced in arid regions of the world, easily causing soil consolidation, fertility decline, and crop yield reduction, which seriously restricts the regional sustainable development [1], [2]. Soil salt content (SSC) is an important research index to evaluate the degree of soil salinization, how to rapidly and accurately obtaining information on SSC is a necessary prerequisite for scientific management and reasonable utilization of saline soil, and also an important basis for effective evaluation of soil salinization [3], [4]. The traditional method of obtaining SSC is fixed-point sampling and measured by conductivity meter, which uses data measured by a conductivity meter; however, this method is time-consuming and laborious, which is not conducive to large-scale monitoring of farmland in irrigation area [5], [6]. Remote sensing has been widely used in soil salinization monitoring [7], [8], [9].

Satellite remote sensing provides a method to quickly monitor soil salinity in a wide range, Sertel [10] focused on multitemporal monitoring of Tuz Lake Region in order to track changes in areas of salty spots by using Landsat-5 TM and Landsat-8 remote sensing images. However, satellite remote sensing is vulnerable to weather and spatial resolution images, and UAV can make up for these problems. UAV technology has become a practical and direct tool for sample acquisition and image information acquisition. Hence, UAV technology has emerged as a practical and straightforward tool for samples collection and image information acquisition [11], [12], [13]. With the close association between spectral signals retrieved from multispectral remote sensing platforms, physicochemical properties of the surface and agriculture, UAV-based data can be used to monitor soil salinization quickly and effectively by establishing salinity inversion models [14], [15], [16], [17].

With the continuous development of remote sensing technology, the combination of UAV remote sensing and algorithms has been widely used for soil salinity inversion [18], [19], [20], which can effectively solve large-scale monitoring issues in salinization process assessment. In this regard, using multispectral UAV to monitor salinity in the topsoil (0–20 cm), Wei [17] established various machine learning models like back propagation neural network (BPNN) and then evaluated and optimized the best salt inversion model. Similarly, Qi [21] extracted spectral reflectance and spectral index based on UAV ground cooperative system and used machine learning algorithms such as BPNN to build a salinity inversion model and the results showed that the established model could reflect the salinization degree in the study area. Most of the models built in the above research are basic BPNN models, which are prone to uncertain

Manuscript received 24 December 2022; revised 5 March 2023 and 19 April 2023; accepted 29 May 2023. Date of publication 8 June 2023; date of current version 11 July 2023. This work was supported in part by the National Natural Science Foundation of China under Grant 51869010, in part by Gansu Youth Science and Technology Fund Program under Grant 21JR7RA778, in part by Gansu Excellent Postgraduate Innovation Star Project under Grant 2022CXZX-446, and in part by Gansu Excellent Postgraduate Innovation Star Project under Grant 2023CXZX-433. *(Corresponding author: Wenju Zhao.)*

Wenju Zhao, Hong Ma, Chun Zhou, and Changquan Zhou are with the Lanzhou University of Technology, Lanzhou 730050, China (e-mail: wenjuzhao@126.com; mahong@lut.edu.cn; zhouchun@lut.edu.cn; 20191110039@lzxk.edu.cn).

Zongli Li is with the Ministry of Water Resources of the Peoples's Republic of China, Beijing 100053, China (e-mail: lizongli@giwp.org.cn).

Digital Object Identifier 10.1109/JSTARS.2023.3284019

local extremum, poor robusticity, slow convergence speed, and convergence accuracy [22], [23], [24].

In this regard, scholars have found that the constructed PSO-BPNN, thinking evolutionary algorithm (MEA)-BPNN, and GA-BPNN models can effectively improve the monitoring accuracy and enhance the robustness of the models [25], [26], [27], [28]. However, the optimization algorithms are mainly widely used in remote sensing image classification and recognition, while less attention has been paid to the use of PSO, MEA, and GA algorithms for optimizing soil salinity monitoring. In view of this, used the UAV multispectral image and field measurements of 60 soil surface salinity as data sources, 16 salinity indexes were constructed using the extracted spectral reflectance, and performed a gray relation analysis (GRA) to screen salt index features after applying a film removal to build the BPNN salinity inversion model. The main objectives of this study are to

1) explore the effectiveness of the GRA to remove redundant information in spectral variables;
2) construct PSO-BPNN, MEA-BPNN, and GA-BPNN models to explore the optimization ability of PSO algorithm, MEA algorithm, and GA algorithm, and improve the robusticity of salinity inversion model;
3) compare and evaluate the optimization performance of the fore state-of-the-art algorithms, and optimize the best optimization algorithm. This research will provide a theoretical foundation for rapid inversion and improved accuracy in soil salinity assessment.

II. Materials and Methods

A. Study Area

The study area is located in Taolai River basin of Hexi Corridor in China. The land in Hexi Corridor is flat contiguous, sufficient light, day and night temperature difference, and unique natural conditions. It is not only an important commodity grain base and crop seed production base in Gansu Province and even the whole northwest region, but also an important reserve land resource area in China. According to the third national land survey, the salinization of soil in Hexi Corridor is becoming more and more serious, with salinized land reaching 1.0679 million hm^2, which the salinized cultivated land accounts for 30.17% of the cultivated land area, and the salinized land develops from speckle to flake. Tao Lai River is a typical soil salinization area in the Black River Basin, which ranges from 98°20′ to 99°18′E and 39°10′ to 40°15′N, with a total area of 0.454 million km^2. The region has an average annual precipitation of 72.6 mm and an average annual evaporation of 2184.0 mm, which is a typical "no irrigation, no agriculture" area (see Fig. 1).

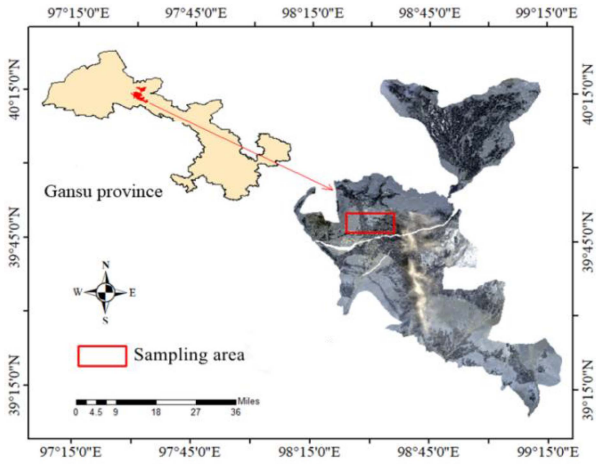

Fig. 1. Study area's geographical location.

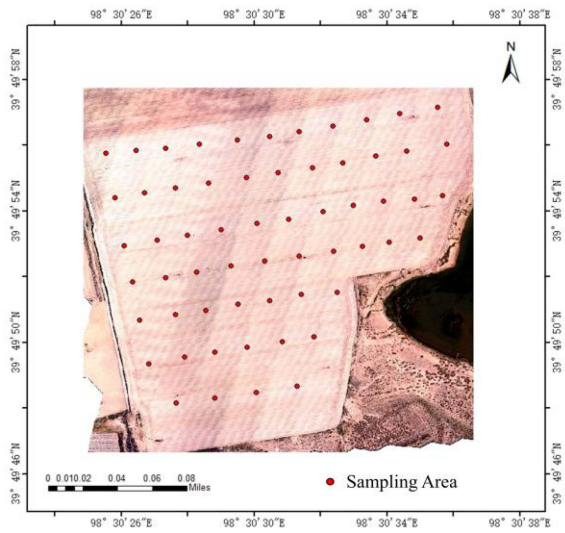

Fig. 2. Sampling sites.

B. Data Acquisition and Analysis

1) Measured Data: The 60 sampling plots were evenly distributed in a representative cultivated land, sampling depths of 0–10 cm. The TRIME method was used to repeatedly measure each sampling point three times, and the average value was taken as the soil salinity. The measurement range of TRIME is 0–10 ms/cm, resolution 0.01 ms/cm, and accuracy ±0.02. To ensure the temporal consistency between the UAV remote sensing images and ground data, sampling was carried out while acquiring multispectral remote sensing images, and the location of each sampling point was recorded by GPS (see Fig. 2).

2) UAV Multispectral Data Acquisition and Preprocessing: The UAV remote sensing platform used in this study is the DJI P4 multispectral version produced by the Da Jiang company, which has a visible light camera and five multispectral cameras (see Table I). The experiment was conducted in Taolai River basin on May 2021 with clear weather and UAV multispectral images acquired between 11:00 and 14:00. The photography mode was equal time interval photography, the interval time was 2 s, the flight speed was 6.8 m/s, the flight height was 100 m, the heading overlap rate was 80%, and the side overlap rate was 70%. The acquired spectra were calibrated with a standard white board before acquisition, and the acquired multispectral images were imported into DJI Wisdom for image correction, cropping, and other preprocessing.

TABLE I
MULTISPECTRAL UAV PARAMETERS

parameter	size
Take-off weight/g	1487
PTZ rotation range /°	-90 °～+ 30 °
Image Resolution	1600×1300
Band and band width /nm	B 450 nm±16 nm
	G 560 nm±16 nm
	R 650 nm±16 nm
	RedEdge 730 nm±16 nm
	NIR 840 nm±26 nm

There is film mulching on cultivated land subsurface over the Taolai River irrigation area. The spectral characteristics of cultivated land after film mulching are different from those of bare soil area. Therefore, film mulching will affect the accuracy of soil salinization monitoring over large areas. The neural network method as a supervised classification technique was applied to remove the film effect on UAV multispectral remote sensing image. The precision of soil salinity inversion is improved by removing the film effect on the film-covered cultivated land [29]. The results are presented in Fig. 3.

C. Calculation of Salinity Indexes

In this article, the soil spectral index is selected as the index of remote sensing evaluation, and the extracted spectral reflectance calculates the salinity index. We introduced the red-edge band and computed sixteen salinity indexes. The salinity indexes are NDSI, NDSI reg, S1, S2, S3, S4, S5, S6, BI, SI1, SI1- reg, SI2, SI2-reg, SI3, SI3-reg, and SI-T, respectively, as shown in Table II.

D. Gray Relation Analysis

This article introduces the GRA method into the gray system analysis of salinization. The GRA method judges whether the relationship between variables is close according to the similarity or difference of development trends between variables [34]. This method makes up for the shortcomings caused by the systematic analysis of mathematical statistics, and it is also applicable to the number of samples and the regularity of samples. Wei [17] used the GRA to screen the variables, and the results showed that the model accuracy of the variables screened by GRA was higher. During the neural network model training, too much input layer data will affect the model's learning process and reduce the model's convergence speed and prediction accuracy. Therefore, the gray correlation analysis method is employed to remove the redundant data in this work

$$\mathrm{GCD} = \frac{1}{n}\sum_{t=1}^{n}\gamma\left(x_0(t), x_i(t)\right) \tag{1}$$

$$\gamma\left(x_0(t), x_i(t)\right) = \frac{\Delta(\min) + \rho\Delta(\max)}{\Delta_{0i}(k) + \rho\Delta(\max)} \tag{2}$$

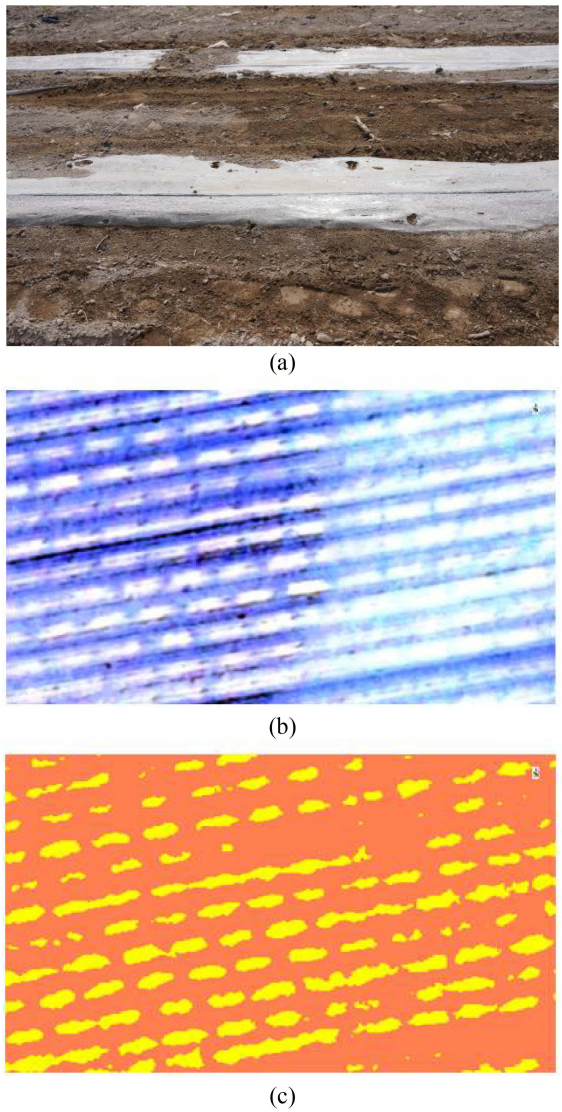

Fig. 3. Comparison of multispectral images before and after film removal. (a) Film mulching image. (b) Before film removal. (c) After film removal.

where ρ is the resolution coefficient, which is taken as 0.5 in this article.

E. Optimistic Algorithm

1) Particle Swarm Optimization (PSO) Algorithm: The core of the PSO algorithm is the collaboration between individuals in the group and the sharing of information [35]. The PSO algorithm optimizes the neural network as follows: determining the feasible domain of the optimization problem, randomly scattering some particles into the feasible domain at the initial moment and assigning an initial random position and an initial random velocity to each particle. Then each particle's position is advanced in turn according to its velocity, the known optimal global position in the problem space, and the known optimal position of the particle. The following is the calculation formula:

$$v_{id}^{t} = \omega \cdot v_{id}^{t-1} + c_1 r_1\left(p_{id}^{t} - x_{id}^{t-1}\right) + c_2 r_2\left(p_{gd}^{t} - x_{id}^{t-1}\right) \tag{3}$$

TABLE II
MATHEMATICAL FORMULAE OF USED SALINITY INDEXES

Salinity Index	Calculation formula	Reference
Normalized Difference Soil Index(NDSI)	NDSI=*(R-NIR)/(R+NIR)*	[30]
Normalized Difference Soil Index−reg(NDSI-reg)	NDSI-reg=*(RedEdge-NIR)/(RedEdge +NIR)*	[31]
Salinity index (S1)	S1=*B/R*	[32]
Salinity index (S2)	S2=*(B-R)/(B+R)*	
Salinity index (S3)	S3=*(G×R)/B*	
Salinity index (S4)	S4=$\sqrt{B \times R}$	
Salinity index (S5)	S5=*(B × R)/G*	
Salinity index (S6)	S6=*(R×NIR)/G*	
Brightness index (BI)	BI=$\sqrt{R^2 + NIR^2}$	[30]
Salinity index1 (SI1)	SI1=$\sqrt{G \times R}$	[33]
Salinity index1-reg (SI1-reg)	SI1-reg=$\sqrt{G \times RedEdge}$	[31]
Salinity index2 (SI2)	SI2=$\sqrt{G^2 + R^2 + NIR^2}$	[33]
Salinity index2-reg (SI2-reg)	SI2=$\sqrt{G^2 + RedEdge^2 + NIR^2}$	[31]
Salinity index3 (SI3)	SI3=$\sqrt{G^2 + R^2}$	[33]
Salinity index3-reg (SI3-reg)	SI3=$\sqrt{G^2 + RedEdge^2}$	[31]
Soil Index-T(SI-T)	SI-T=*100(R-NIR)*	

Note: the band lengths of B, G, R, NIR and Red-edge are 450, 560, 650, 840, and 730 nm, respectively.

where c_1 and c_2 are social learning factors and individual learning factors, r_1 and r_2 are random functions with the value range of [0, 1] to increase the randomness of the search, and ω is the inertia weight to adjust the search range of the space.

2) Mind Evolutionary Algorithm: The mind evolutionary algorithm is a process of imitating the evolution of human thinking [36]. It inherits the ideas of "group" and "evolution" of genetic algorithm (GA) and makes major innovations. The group is divided into several subgroups, and the "convergence" and "alienation" operators are proposed, which has strong global optimization ability. The specific steps of the MEA are as follows.

1) *Group initialization:* Determine the size of the group N and the number of subgroups $M = N_S + N_T$, N_S represents the number of superior subgroups, N_T represents the number of temporary subgroups. N individuals are randomly generated in the solution space, and their scores are calculated to select M winners.
2) *Convergence process:* Create new subgroups guided by the information of each winner. Within each subgroup, individual scores are calculated, with the highest score being the winner and representing the score for that subgroup. Record the winner's information to the global bulletin board and local bulletin board. The remaining individuals learn from the winner in a certain way, generating new subgroups, repeating the above steps until the subgroups mature.
3) *Alienation process:* At each step of evolution, there is global competition among all subpopulations. The subpopulations that lost their competitive ability were eliminated, and under the guidance of environmental knowledge and evolutionary information, an equal number of new subpopulations were regenerated in the solution space and reparticipated in the global competition.

Repeat the above-mentioned steps until the score of the best subgroup is not further improved. The following is the calculation formula:

$$\{f_k^*\} = \{f_*(0), f_*(1), f_*(2), \ldots, f_*(k), \ldots\} \tag{4}$$

where k is a positive integer representing evolutionary algebra, and $f_*(k) \leq f_*(k-1)$.

3) Genetic Algorithm: GA is an evolutionary process on a randomly selected population [37]. In the evolutionary process of GA, each individual in the population records its fitness measure according to a defined cost function. This process mimics natural selection and natural evolution, effectively improving the outcome of the solution. In the GA feature extraction stage, it is necessary to select the best attribute to represent the data set of the problem, which is determined by the fitness function defined for the problem. The following is the fitness function:

$$F = k \cdot \left[\sum_{i=1}^{L} abs(y_i - o_i)\right] \tag{5}$$

where L is the number of individual samples, y_i is the expected output of the ith individual of the neural network, o_i is the predicted output of the ith individual, and k is the coefficient.

F. Model Accuracy Evaluation

Model accuracy assessment was conducted using the determination coefficient (R^2), root mean square error (RMSE), and performance deviation ratio (RPD). The larger the value of R^2 is, the lower the *RMSE* value is, and the more accurate model is [17]. The RPD was classified into three groups denoted as follows: class A (RPD $>$ 2.0), class B (1.40 $\leq$ RPD $\leq$ 2.0), and class C (RPD $<$ 1.40). Evaluation metrics can be computed using (6), (7), and (8)

$$R^2 = \sum_{i=1}^{n} (\hat{y}_i - \overline{y_i})^2 / \sum_{i=1}^{n} (y_i - \overline{y_i})^2 \tag{6}$$

$$\text{RMSE} = \sqrt{\sum_{i=1}^{n} (\hat{y}_i - \overline{y_i})^2 / n} \tag{7}$$

$$\text{RPD} = \sqrt{\sum_{i=1}^{n} \bar{V}(y_i)^2 / n} \Big/ \text{RMSE} \tag{8}$$

where $\hat{y}_i$, y_i, and $\bar{y}_i$ denote the predicted, measured, and average measured values of SSC, respectively; n is the number of samples.

TABLE III
STATISTICAL ANALYSIS OF SOIL SALINITY

Sample set	Sample size					salinity			
	Sample	None salinization	Mild salinization	Moderate salinization	Severe salinization	Maximum	Minimum	Mean	C_V
Total sample	60	6	33	14	7	1.94	0.43	0.73	0.49
Training set	40	4	23	9	4	1.87	0.43	0.72	0.46
Test set	20	2	10	4	3	1.94	0.52	0.74	0.49

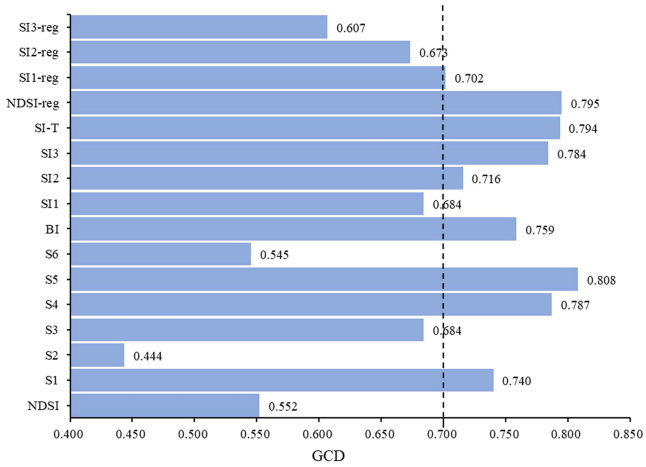

Fig. 4. GCD analysis result.

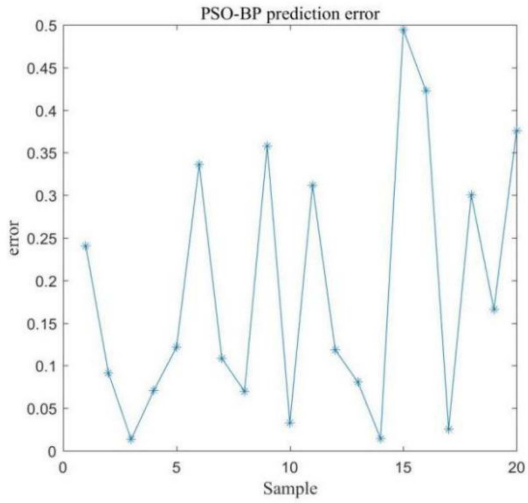

Fig. 5. PSO-BPNN prediction error.

III. RESULTS AND ANALYSIS

A. Statistical Analysis of Soil Salinity

The 60 samples of SSC measured are divided into four grades, none saline soil, mild salinization, moderate salinization, and severe salinization. The analysis of the distribution of the number of samples of SSC is shown in Table III. According to the statistical results, the proportion of none saline soil, mild saline soil, moderate saline soil, and severe saline soil in the total sample number is 10%, 55%, 23.3%, and 11.7%, and the coefficient of variation is 0.49, showing moderate variability; among them, moderately salinized soil accounts for the largest proportion. Because the SSC in the study area did not change much during the year, the SSC in May was taken as an example.

B. GRA and Algorithm Optimization Process

The correlation between salinity indexes and SSC was analyzed by gray relational analysis in MATLAB R2016a (see Fig. 4). In order to achieve the purpose of sensitive variable screening, the screening threshold of GCD was set to 0.7, and the sensitive spectral indexes screened by GRA were S1, S4, S5, BI, SI2, SI3, SI-T, NDSI-reg, and SI1-reg.

The PSO-BPNN prediction error is shown in Fig. 5; the subpopulation convergence process of MEA-BPNN algorithm is divided into temporary subpopulation and superior subpopulation, as shown in Fig. 6(a) and (b); the fitness curve of GA-BPNN algorithm is shown in Fig. 7, and the termination algebra is 50.

C. Methodological Workflow

Based on UAV multispectral remote sensing data and field measurements, this study uses GRA to screen variables and establish BPNN model, optimize it by PSO algorithm, MEA algorithm, and GA algorithm, compare the accuracy of the optimization model, and select the best soil salt inversion model. The flow method of this study is shown in Fig. 8 in order to provide a clearer idea for researchers.

D. Salt Content Inversion BPNN Model Based on Three Different Optimization Algorithms

The salt content inversion model is created using BPNN, MEA-BPNN, PSO-BPNN, and GA-BPNN algorithms. After gray correlation analysis, independent variables associated with soil salinity were selected for the model's input layer, while the output layer refers to the corresponding salt content values. Table IV shows the accuracy comparison of the inversion results of the four models. The scatter diagram of predicted values using the four models is presented in Fig. 9.

Among the determination coefficient R^2 results based on the training set, the GA-BPNN model is the best fit with a value of 0.6573. Overall, RMSE values of the training set are the lowest; hence, for the optimized three models, they are below

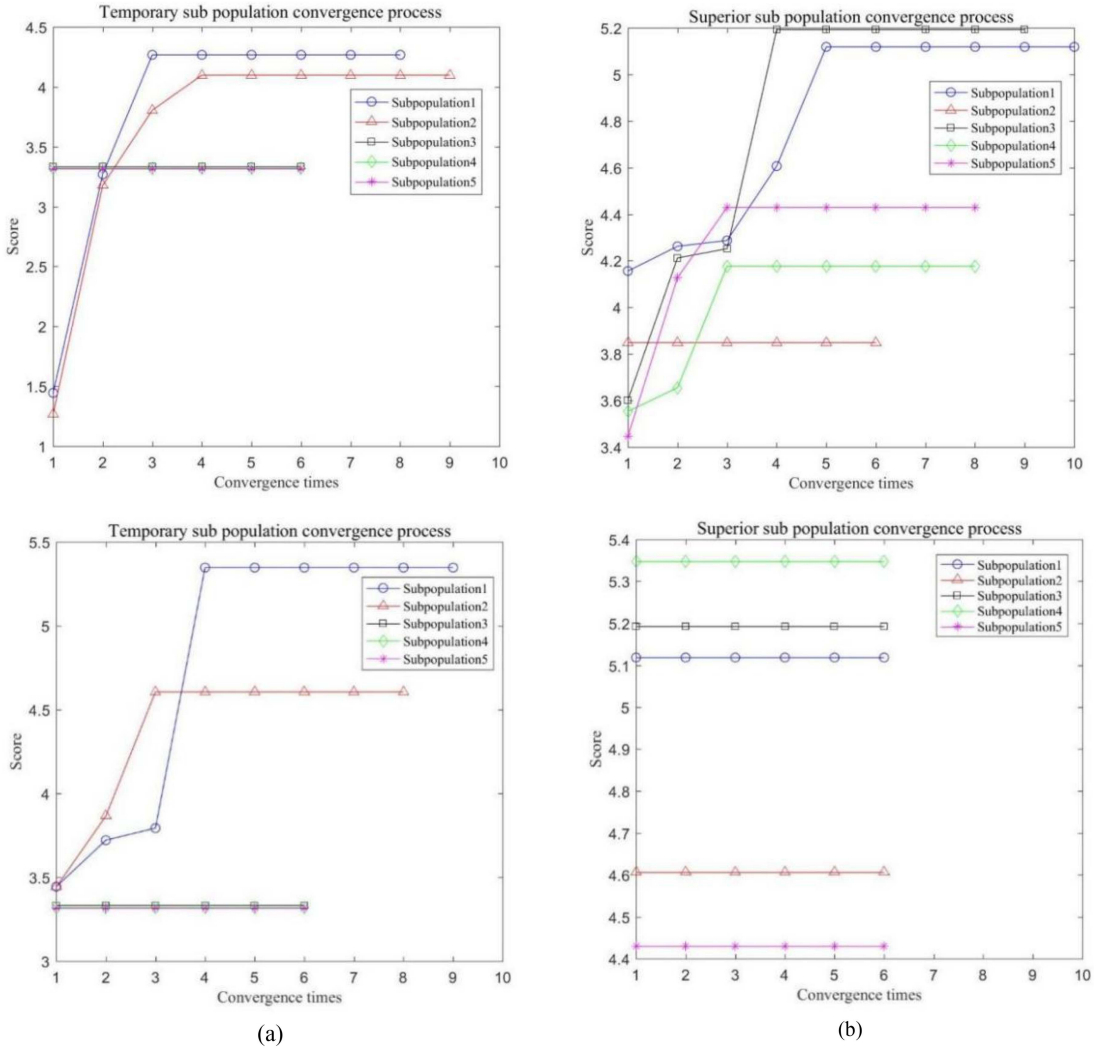

Fig. 6. MEA subpopulation convergence process. (a) MEA temporary subpopulation convergence process. (b) MEA superior subpopulation convergence process.

TABLE IV
INVERSION MODEL BASED ON SALINITY INDEXES

Model	Training set		Testing set		RPD
	R^2	RMSE/%	R^2	RMSE/%	
BPNN	0.3792	0.1623	0.3912	0.1232	1.4221
PSO-BPNN	0.3970	0.1411	0.4102	0.1123	1.5433
MEA-BPNN	0.4901	0.1170	0.5330	0.1092	1.7912
GA-BPNN	0.6573	0.1042	0.6659	0.0751	2.0211

0.15%, with the outperformance GA-BPNN model (RMSE = 0.104%). For the test set, R^2 is slightly higher than that of the training set, while RMSE is lower than that of the training set, indicating the superiority of the inversion effect for the four models during the testing phase. For the test set of the three optimized models, the GA-BPNN model has the best inversion effect with a coefficient of determination R^2 of 0.6659, an RMSE value of 0.0751%, and an RPD value of 2.0211 (class A). The MEA-BPNN model also achieved an acceptable inversion effect, with an RPD value of 1.7912 (class B). The PSO-BPNN is the least performant, followed by the initial BP model in terms of the inversion effect. Fig. 9 illustrates the estimated and measured salt content values for the four prediction models. It can be observed from Table IV and Fig. 9. that the optimized BPNN model, whether using PSO, MEA, or GA algorithms, can effectively improve the inversion accuracy of salinity estimation.

Fig. 10 illustrates the measured and predicted values of the four models. Comprehensive analysis of Fig. 9 and Table IV revealed that compared to the nonoptimized BPNN model, the determination coefficient of the model test set after PSO optimization was increased by 0.019, the RMSE was reduced by 0.0109%, and the RPD has increased by 0.1212. For MEA optimization, the determination coefficient of the initial model was increased by 0.1418, the RMSE was reduced by 0.014%, and the RPD was increased by 0.3691. For GA optimization, the determination coefficient was increased by 0.2747. The RMSE was reduced by 0.0481%, while the RPD was increased by 0.599. Compared to the MEA-BPNN model, the determination coefficient of the GA-BPNN model was increased by 0.1329, the

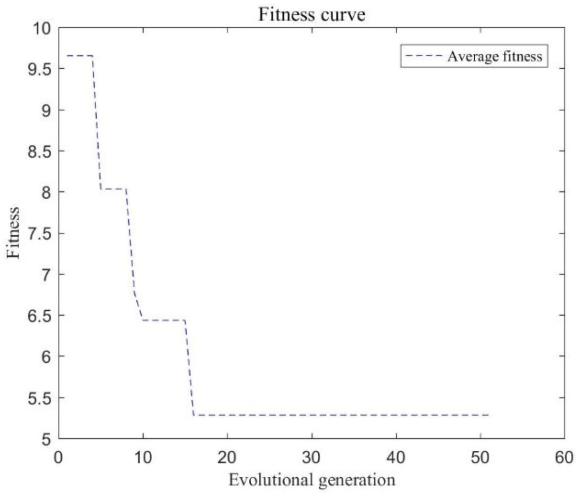

Fig. 7. GA-BPNN fitness curve.

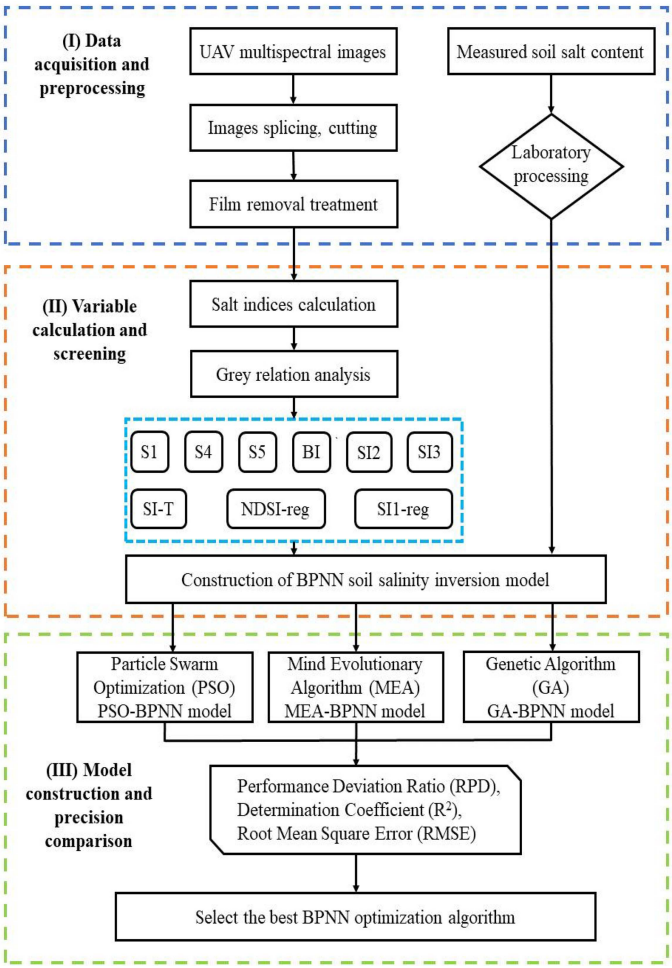

Fig. 8. Methodological workflow.

RMSE was reduced by 0.0341%, and the RPD was increased by 0.2299. Compared to the PSO-BPNN model, the determination coefficient of the GA-BPNN model was increased by 0.2557, the RMSE was reduced by 0.0372%, and the RPD was increased by 0.4778. Based on Fig. 10, the GA-BPNN model is the best fit for soil salinity prediction, followed by the MEA-BPNN model and PSO-BPNN model with the lowest optimization effect. The results revealed that the BPNN model optimized by the GA is the most performant salinity inversion model.

The SSC in the study area based on the GA-BPNN model inversion is shown in Fig. 11. As shown in Fig. 11, it can be seen that the degree of salinization in the study area is relatively heavy, and the inversion results are in line with the actual situation of the study area, which can provide a theoretical basis for the effective prevention and control of soil salinization in this area.

IV. Discussion

UAV remote sensing has the advantages of high timeliness and convenience [38]. It can be used for large-scale and rapid monitoring of soil salinization on the farm scale [39], which is revolutionary progress toward agricultural informatization in the future [40], [41], [42]. Similarly, Hu et al. [15] has estimated field-scale soil salinity using electromagnetic induction instrument coupled with a hyperspectral camera installed on a UAV platform. The results indicated that a UAV-borne hyperspectral imager is a valuable tool for field-scale soil salinity monitoring and mapping as well. Based on spectral index fusion of high-spatial-resolution and low-spatial-resolution remote sensing data, Ma [16] has established a soil salinity inversion model with high accuracy. The study investigated the efficiency of UAV multispectral data for salt information extraction over heavy saline lands. Our research removed film-mulched cultivated land, and then significant variables were selected through the gray correlation analysis method. The soil salt inversion model is created based on the UAV multispectral remote sensing image, which improves the efficiency and accuracy of salinization monitoring in the arid oasis area of Northwest China.

This article uses the optimization algorithm to solve the BPNN and establish the optimization model. Many scholars have done similar research like Wang [43]. Wang [44] and Cao [45] constructed a temperature drift compensation model of BPNN optimized by a mind evolutionary algorithm. The results showed that the MEA algorithm could explore the BP network for better threshold and connection weight to improve the model's compensation effect. In this work, the BPNN model is optimized by the MEA algorithm to estimate salt content; hence a better inversion performance is obtained. Ismail [14] combined PSO with the BP algorithm and proposed a robust hybrid training algorithm with acceptable accuracy with local and global search capabilities. Based on the inversion model accident source term of BPNN, Ling [46] investigated the issues of BPNN like local minima during the training process. The study used a GA to optimize the weight and threshold of BPNN, which improves the training rate of the BPNN and achieves a better optimization effect with higher accuracy. This supports our findings regarding the GA optimization method's superiority for prediction. By comparing the soil salt inversion accuracy of the three optimization algorithm models, GA algorithm optimizing effect for BPNN was improved than the MEA algorithm. Due to the small sample size for testing, the PSO algorithm can end up falling into the local optimal solution. Therefore,

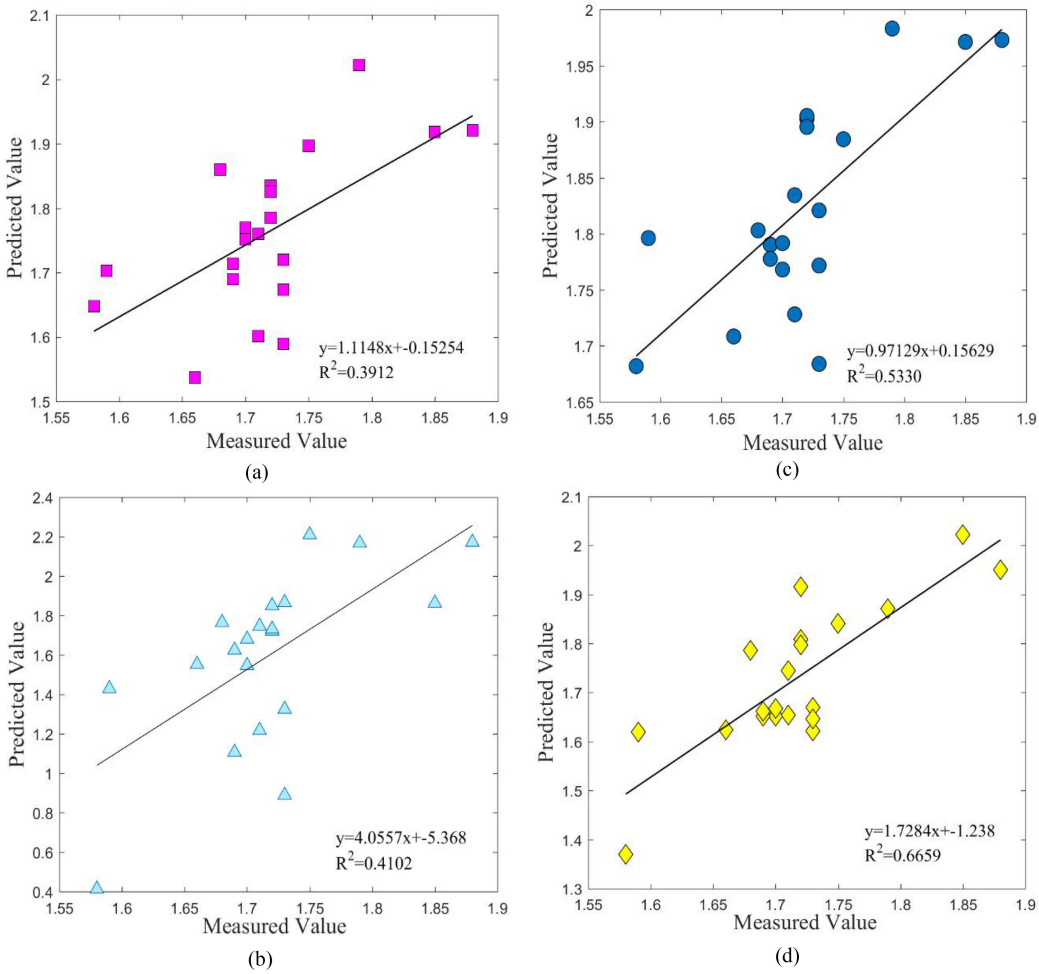

Fig. 9. Scatter diagram of predictive models. (a) BPNN model. (b) PSO-BPNN model. (c) MEA-BPNN model. (d) GA-BPNN model.

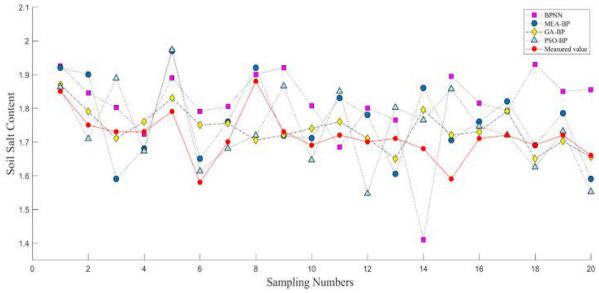

Fig. 10. Comparison between the measured value and predicted values.

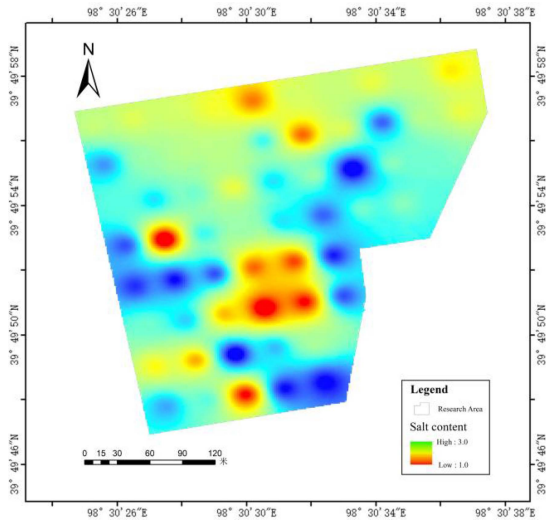

Fig. 11. SSC map based on the GA-BPNN model.

its performance was slightly mediocre than the other two algorithms.

Although only UAV multispectral remote sensing images were used with a small size of reference data, the soil salt inversion models established based on the BPNN optimization algorithm have achieved acceptable inversion accuracy. Multisource remote sensing data fusion can further improve the accuracy of salinity inversion models [47], [48]. A deep-learning algorithm can also effectively solve the generalization issues of limited sample datasets [49], [50]. In future research, we will complete the application of the model in a larger regional scale, investigate retrieving farmland soil salt by multisource remote sensing scale conversion based on a depth learning algorithm,

improve the computational power of the inversion model, and provide a theoretical basis for digital agriculture.

V. Conclusion

Used the UAV multispectral image and field measurements of 60 soil surface salinity as data sources, 16 salinity indexes were constructed using the extracted spectral reflectance, and performed a GRA to screen salt index features after applying a film removal to build the BPNN salinity inversion model. PSO, MEA, and GA were applied to optimize the BPNN inverse model, respectively, and the optimization capabilities of the four algorithms were compared and evaluated to optimize the best optimization algorithm. The main conclusions are as follows.

1) The GRA variable screening can effectively remove the redundant information in the spectral variables, reduce the complexity of model building. The number of sensitive spectral indices screened by the GRA variable screening was nine.
2) The PSO algorithm, MEA algorithm, and GA algorithm can effectively improve the robusticity of the salinity inversion model, and the GA algorithm is the best optimization algorithm.
3) The accuracy of the PSO-BPNN, MEA-BPNN, and GA-BPNN inversion models are better than that of the BPNN model, and GA-BPNN is the best salinity inversion model, which achieves R^2 of 0.6659, RMSE of 0.0751, and RPD of 2.0211. Compared with the MEA-BPNN and PSO-BPNN models, the determination coefficient of the GA-BPNN model was increased by 0.1329 and 0.2557, the RMSE was reduced by 0.0341% and 0.0372%, and the RPD was increased by 0.2299 and 0.4778.

References

[1] X. Fan, X. Zhao, Y. Liu, R. Guo, and Y. Liu, "Soil salinity dynamics impairs radiometer-based soil moisture retrieval over global cropland," *IEEE Trans. Geosci. Remote Sens.*, vol. 60, 2022, Art. no. 5304309, doi: 10.1109/TGRS.2022.3181586.

[2] A. Samet, Y. Aylin, G. Taha, H. Nikou, T. Aysegul, and S. Elif, "Assessing the performance of machine learning algorithms for soil salinity mapping in Google Earth Engine platform using Sentinel-2A and Landsat-8 OLI data," *Adv. Space Res.*, vol. 69, no. 2, pp. 1072–1086, 2022.

[3] K. Ivushkin, H. Bartholomeus, A. K. Bregt, A. Pulatov, B. Kempen, and L. D. Sousa, "Global mapping of soil salinity change," *Remote Sens. Environ.*, vol. 231, 2019, Art. no. 111260.

[4] F. Wang, Z. Shi, A. Biswas, S. Yang, and J. Ding, "Multi-algorithm comparison for predicting soil salinity," *Geoderma*, vol. 365, 2019, Art. no. 114211.

[5] P. Jin, P. Li, Q. Wang, and Z. Pu, "Developing and applying novel spectral feature parameters for classifying soil salt types in arid land," *Ecological Indicators*, vol. 54, pp. 116–123, 2015.

[6] W. Zhao, C. Zhou, C. Zhou, H. Ma, and Z. Wang, "Soil salinity inversion model of oasis in arid area based on UAV multispectral remote sensing," *Remote Sens.*, vol. 14, 2022, Art. no. 1804.

[7] H. Shi et al., "A global meta-analysis of soil salinity prediction integrating satellite remote sensing, soil sampling, and machine learning," *IEEE Trans. Geosci. Remote Sens.*, vol. 60, 2022, Art. no. 4505815, doi: 10.1109/tgrs.2021.3109819.

[8] S. Wang, Y. Chen, M. Wang, Y. Zhao, and J. Li, "SPA-based methods for the quantitative estimation of the soil salt content in saline-alkali land from field spectroscopy data: A case study from the yellow river irrigation regions," *Remote Sens.*, vol. 11, no. 8, 2019, Art. no. 967.

[9] L. Wang et al., "Estimation of soil salt and ion contents based on hyperspectral remote sensing data: A case study of baidunzi basin, China," *Water*, vol. 13, no. 4, pp. 559–559, 2021.

[10] E. Sertel, T. Gorji, and A. Tanik, "Monitoring soil salinity via remote sensing technology under data scarce conditions: A case study from Turkey," *Ecological Indicators*, vol. 74, pp. 384–391, 2017.

[11] J. Farifteh, A. Farshad, and R. J. George, "Assessing salt-affected soils using remote sensing, solute modelling, and geophysics," *Geoderma*, vol. 130, no. 3, pp. 191–206, 2005.

[12] C. Romero-Trigueros et al., "Effects of saline reclaimed waters and deficit irrigation on Citrus physiology assessed by UAV remote sensing," *Agricultural Water Manage.*, vol. 183, pp. 60–69, 2017.

[13] W. S. Seung, W. K. Dong, G. S. Woong, and J. Y. Jae, "Integrating UAV and TLS approaches for environmental management: A case study of a waste stockpile area," *Remote Sens.*, vol. 12, no. 10, 2020, Art. no. 1615.

[14] A. Ismail, D. S. Jeng, and L. L. Zhang, "An optimised product-unit neural network with a novel PSO-BPNN hybrid training algorithm: Applications to load-deformation analysis of axially loaded piles," *Eng. Appl. Artif. Intell.*, vol. 26, no. 10, pp. 2305–2314, 2013.

[15] J. Hu et al., "Quantitative estimation of soil salinity using uav-borne hyperspectral and satellite multispectral images," *Remote Sens.*, vol. 11, no. 7, 2019, Art. no. 736.

[16] Y. Ma, H. Chen, G. Zhao, Z. Wang, and D. Wang, "Spectral index fusion for salinized soil salinity inversion using sentinel-2A and UAV images in a coastal area," *IEEE Access*, vol. 8, pp. 159595–159608, 2020, doi: 10.1109/ACCESS.2020.3020325.

[17] G. Wei, Y. Li, Z. Zhang, and Y. Chen, "Estimation of soil salt content by combining uav-borne multispectral sensor and machine learning algorithms," *Peer J.*, vol. 8, no. 2, 2020, Art. no. e9087.

[18] A. Aldabaa, D. C. Weindorf, S. Chakraborty, A. Sharma, and B. Li, "Combination of proximal and remote sensing methods for rapid soil salinity quantification," *Geoderma*, vol. 239, pp. 239–240, 2015.

[19] X. Fan, Y. Liu, J. Tao, and Y. Weng, "Soil salinity retrieval from advanced multi-spectral sensor with partial least square regression," *Remote Sens.*, vol. 7, pp. 488–511, 2015.

[20] X. Xu, Y. Chen, M. Wang, S. Wang, K. Li, and Y. Li, "Improving estimates of soil salt content by using two-date image spectral changes in Yinbei, China," *Remote Sens.*, vol. 13, no. 20, pp. 4165–4165, 2020.

[21] G. Qi, G. Zhao, and X. Xi, "Soil salinity inversion of winter wheat areas based on satellite-unmanned aerial vehicle-ground collaborative system in coastal of the yellow river delta," *Sensors*, vol. 20, no. 22, pp. 6521–6521, 2021.

[22] J. Dong, W. Qin, and J. Mo, "Low-cost multi-objective optimization of multiparameter antenna structures based on the l1 optimization BPNN surrogate model," *Electronics*, vol. 8, no. 8, p. 839, 2019.

[23] J. Fei, Z. Wu, X. Sun, D. Su, and X. Bao, "Research on tunnel engineering monitoring technology based on BPNN neural network and MARS machine learning regression algorithm," *Neural Comput. Appl.*, vol. 33, no. 1, pp. 1–17, 2020.

[24] P. Jia, T. Shang, J. Zhang, and S. Yuan, "Inversion of soil pH during the dry and wet seasons in the Yinbei region of Ningxia, China, based on multi-source remote sensing data," *Geoderma Regional*, vol. 25, 2021, Art. no. e00399.

[25] W. C. Chen and D. Kurniawan, "Process parameters optimization for multiple quality characteristics in plastic injection molding using Taguchi method, BPNN, GA, and hybrid PSO-GA," *Int. J. Precis Eng. Manuf.*, vol. 15, no. 8, pp. 1583–1593, 2014.

[26] Y. Yang, G. Wang, and Y. Yang, "Parameters optimization of polygonal fuzzy neural networks based on GA-BPNN hybrid algorithm," *Int. J. Mach. Learn. Cybern.*, vol. 5, no. 5, pp. 815–822, 2014.

[27] S. Wang, N. Zhang, L. Wu, and Y. Wang, "Wind speed forecasting based on the hybrid ensemble empirical mode decomposition and GA-BPNN neural network method," *Renewable Energy*, vol. 94, pp. 629–636, 2016.

[28] Z. Meng et al., "Prediction method of driving strategy of high-power IGBT module based on MEA-BPNN neural network," *IEEE Access*, vol. 8, pp. 94731–94747, 2020, doi: 10.1109/ACCESS.2020.2995601.

[29] J. Farifteh, F. vander Meer, and E. J. M. Carranza, "Similarity measures for spectral discrimination of salt-affected soils," *Int. J. Remote Sens.*, vol. 28, no. 23, pp. 5273–5293, 2007.

[30] N. M. Khan, V. V. Rastoskuev, Y. Sato, and S. Shiozawa, "Assessment of hydrosaline land degradation by using a simple approach of remote sensing indicators," *Agricultural Water Manage.*, vol. 77, no. 1-3, pp. 96–109, 2005.

[31] S. Zhang et al., "Integrated satellite, unmanned aerial vehicle (UAV) and ground inversion of the SPAD of winter wheat in the reviving stage," *Sensors*, vol. 19, no. 7, 2019, Art. no. 1485.
[32] A. Allbed, L. Kumar, and P. Sinha, "Soil salinity and vegetation cover change detection from multi-temporal remotely sensed imagery in Al Hassa Oasis in Saudi Arabia," *Geocarto Int.*, vol. 33, no. 8, pp. 830–846, 2018.
[33] A. Douaou, H. Nicolas, and C. Walter, "Detecting salinity hazards within a semiarid context by means of combining soil and remote-sensing data," *Geoderma*, vol. 134, no. 1-2, pp. 217–230, 2017.
[34] W. Wang, R. Tang, C. Li, P. Liu, and L. Luo, "A BP neural network model optimized by Mind Evolutionary Algorithm for predicting the ocean wave heights," *Ocean Eng.*, vol. 162, no. 15, pp. 98–107, 2018.
[35] Q. Guo, H. Wu, H. Jin, G. Yang, and X. Wu, "Remote sensing inversion of suspended matter concentration using a neural network model optimized by the partial least squares and particle swarm optimization algorithms," *Sustainability*, vol. 14, no. 4, 2022, Art. no. 2221.
[36] X. Wang et al., "A back propagation neural network model optimized by mind evolutionary algorithm for estimating Cd, Cr, and Pb concentrations in soils using Vis-NIR diffuse reflectance spectroscopy," *Appl. Sci.*, vol. 10, no. 1, 2019, Art. no. 51.
[37] L. Wang, P. Wang, S. Liang, Y. Zhu, J. Khan, and S. Fang, "Monitoring maize growth on the North China plain using a hybrid genetic algorithm-based back-propagation neural network model," *Comput. Electron. Agriculture*, vol. 170, 2020, Art. no. 105238.
[38] J. B. Sankey et al., "Quantifying plant-soil-nutrient dynamics in rangelands: Fusion of UAV hyperspectral-LiDAR, UAV multispectral-photogrammetry, and ground-based LiDAR-digital photography in a shrub-encroached desert grassland," *Remote Sens. Environ.*, vol. 253, 2021, Art. no. 112223.
[39] A. Bhardwaj, L. Sam, F. J. Martín-Torres, and R. Kumar, "UAVs as remote sensing platform in glaciology: Present applications and future prospects," *Remote Sens. Environ.*, vol. 175, pp. 196–204, 2016.
[40] H. Xiang and T. Lei, "Development of a low-cost agricultural remote sensing system based on an autonomous unmanned aerial vehicle (UAV)," *Biosyst. Eng.*, vol. 108, no. 2, pp. 174–190, 2011.
[41] K. P. Rajesh, Y. Vinod, and J. Ramkumar, "Modelling and multi-response optimization of hole sinking electrical discharge micromachining of titanium alloy thin sheet," *J. Mech. Sci. Technol.*, vol. 28, no. 2, pp. 653–661, 2014.
[42] A. R. Catur, "The potential of UAV-based remote sensing for supporting precision agriculture in Indonesia," *Procedia Environ. Sci.*, vol. 24, pp. 245–253, 2015.
[43] X. Wang, F. Zhang, H. Kun, and V. Johnson, "New methods for improving the remote sensing estimation of soil organic matter content (SOMC) in the Ebinur Lake Wetland national nature reserve (ELWNNR) in Northwest China," *Remote Sens. Environ.*, vol. 218, pp. 104–118, 2018.
[44] Z. Wang, G. Ma, D. Gong, J. Sun, and D. Zhang, "Application of mind evolutionary algorithm and artificial neural networks for prediction of profile and flatness in hot strip rolling process," *Neural Process. Lett.*, vol. 50, no. 3, pp. 2455–2479, 2019.
[45] H. Cao et al., "Dual mass MEMS gyroscope temperature drift compensation based on TFPF-MEA-BPNN algorithm," *Sensor Rev.*, vol. 41, no. 2, pp. 162–175, 2021.
[46] Y. Ling, C. Chai, W. Hou, D. Hei, S. Qing, and W. Jia, "A new method for nuclear accident source term inversion based on GA-BPNNNN algorithm," *Neural Netw. World*, vol. 29, no. 2, pp. 71–82, 2019.
[47] Y. Tong, H. Zhou, and L. Jiang, "Exploring the transition effects of foreign direct investment on the eco-efficiency of Chinese cities: Based on multi-source data and panel smooth transition regression models," *Ecological Indicators*, vol. 121, no. 2, 2020, Art. no. 107073.
[48] M. Liu et al., "Comparison of multi-source satellite images for classifying marsh vegetation using DeepLabV3 plus deep learning algorithm," *Ecological Indicators*, vol. 125, no. 11, 2021, Art. no. 107562.
[49] Y. Lecun, Y. Bengio, and G. Hinton, "Deep learning," *Nature*, vol. 521, no. 7553, pp. 436–444, 2015.
[50] A. Zeggada, F. Melgani, and Y. Bazi, "A deep learning approach to UAV image multilabeling," *IEEE Geosci. Remote Sens. Lett.*, vol. 14, no. 5, pp. 694–698, May 2017, doi: 10.1109/LGRS.2017.2671922.

Wenju Zhao born in May 1981, 2009. He received the Graduate degree in agricultural water and soil engineering national key disciplines from Northwest A & F University, Xianyang, China, and the Ph.D. degree in engineering, mainly engaged in cold and arid areas of ecological water conservancy, digital irrigation, and other aspects of research.

He presided over the completion of projects such as the National Natural Science Foundation of China, Gansu Provincial Party Committee Organization Department Long Yuan Young Talent Project and Gansu Provincial Department of Education projects more than 20, published more than 100 academic papers, including more than 50 SCI, EI indexed papers, applied for more than 10 national invention patents, applied for authorization of computer software copyright 1.

Dr. Zhao is a peer reviewer of the National Natural Science Foundation of China, a degree reviewer of the Center for Academic Degrees and Postgraduate Education Development of the Ministry of Education, an evaluation expert of the Quality Assessment Center for Higher Education of the Ministry of Education, a director of the China Water Resources Education Association, a member of the Ecological Water Resources Engineering Committee of the China Water Resources Society, an expert of the Gansu Province Yellow River Basin Ecological Protection and Quality Development Expert Pool, and an expert of the Gansu Provincial Department of Science and Technology, the Hebei Provincial Department of Science and Technology, and the Gansu Provincial Department of Water Resources.

Hong Ma, photograph and biography not available at the time of publication.

Chun Zhou, photograph and biography not available at the time of publication.

Changquan Zhou, photograph and biography not available at the time of publication.

Zongli Li, photograph and biography not available at the time of publication.